Biophysical Journal
Article

Biophysical Society

Action of Antimicrobial Peptides on Bacterial and Lipid Membranes: A Direct Comparison

Joseph E. Faust,[1] Pei-Yin Yang,[1] and Huey W. Huang[1,*]
[1]Department of Physics and Astronomy, Rice University, Houston, Texas

ABSTRACT The bacterial membrane represents an attractive target for the design of new antibiotics to combat widespread bacterial resistance. Understanding how antimicrobial peptides (AMPs) and other membrane-active agents attack membranes could facilitate the design of new, effective antimicrobials. Despite intense study of AMPs on model membranes, we do not know how well the mechanism of attack translates to real biological membranes. To that end, we have characterized the attack of AMPs on *Escherichia coli* cytoplasmic membranes and directly compared this action to model membranes. AMPs induce membrane permeability in *E. coli* spheroplasts or giant unilamellar vesicles (GUVs) under well-defined concentrations of AMPs and fluorescent molecules. The action of AMPs on spheroplasts is unique in producing an intracellular fluorescence intensity time curve that increases in a sigmoidal fashion to a steady state. This regular pattern is reproducible by melittin, LL37, and alamethicin but not by CCCP or daptomycin, agents known to cause ion leakage. Remarkably, a similar pattern was also reproduced in GUVs. Indeed the steady-state membrane permeability induced by AMPs is quantitatively the same in spheroplasts and GUVs. There are, however, interesting dissimilarities in details that reveal differences between bacterial and lipid membranes. Spheroplast membranes are permeabilized by a wide range of AMP concentrations to the same steady-state membrane permeability. In contrast, only a narrow range of AMP concentrations permeabilized GUVs to a steady state. Tension in GUVs also influences the action of AMPs, whereas the spheroplast membranes are tensionless. Despite these differences, our results provide a strong support for using model membranes to study the molecular interactions of AMPs with bacterial membranes. As far as we know, this is the first time the actions of AMPs, on bacterial membranes and on model membranes, have been directly and quantitatively compared.

INTRODUCTION

Ever since the underlying structure of biological membranes was recognized as a lipid bilayer (1,2), bilayers of various lipid compositions have been used as models for studying the property of cell membranes (3). Model membranes typically lack the lipid complexity, leaflet asymmetry, protein content, and membrane reservoirs present in cell membranes, so the validity of these simple models is often unknown. Specifically, there have been questions about the mechanisms of molecular agents that attack cell membranes. Gene-encoded self-defense antimicrobial peptides (AMPs) (4) are one class of bactericides that kill bacteria by permeabilizing the cell's cytoplasmic membranes. There are other classes of antimicrobial agents such as daptomycin (5) and amphotericin B (6) that appear to operate with different modes of membrane-permeabilization other than AMPs. It is of great interest to understand the mechanisms of these membrane-acting antimicrobials for they represent possible alternatives to the conventional antibiotics whose efficacy has been threatened by bacterial resistance. Understanding membrane permeabilization mechanisms may also facilitate gene and drug delivery. However, because of the difficulty and anticipated complications for discerning the action of molecular agents attacking live cell membranes (4,7–11), most AMP studies have been performed with model membranes. The question is: are the mechanisms gleaned from the model membrane studies applicable to cell membranes? Here we try to answer this question by a direct and quantitative comparison of the action of AMPs on *Escherichia coli* spheroplast cytoplasmic membranes and lipid bilayers.

Membrane permeability of unilamellar lipid vesicles, as measured by molecular influx or efflux, can report on the action of AMPs. This is most commonly done by filling vesicles with a membrane-impermeant fluorescent dye and measuring the dye efflux. The time curve for the dye release is typically measured from a single giant vesicle, commonly called a giant unilamellar vesicle (GUV) or

Submitted November 16, 2016, and accepted for publication March 3, 2017.
*Correspondence: hwhuang@rice.edu
Editor: Paulo Almeida.
http://dx.doi.org/10.1016/j.bpj.2017.03.003

from a population of small vesicles. However, the membrane permeability induced by AMPs in solution most likely changes with time, as the peptides gradually bind to the membrane. A single time curve of efflux or influx does not reveal such time-dependent changes. If it is the collective efflux from a population of small vesicles, the kinetics can be complicated by the ensemble average and by the molecular exchange between vesicles by collision (12–14). In addition, how closely the efflux of dye from vesicle membranes represent the action on cell membranes is unknown.

In a recent article (15), we introduced a method for measuring instantaneous permeability through an *E. coli* cytoplasmic membrane as the cell was attacked by AMPs. We removed the outer membranes from *E. coli*, i.e., transformed the cells into spheroplasts, so that AMPs could interact directly with the cytoplasmic membranes. We employed a method of balancing the transmembrane fluxes with photobleaching (previously we used the common term "fluorescence recovery after photobleaching") (15) to monitor the changing state of membrane permeability. Here we apply this method to study spheroplasts and GUVs under the same conditions, using a well-controlled flow chamber.

In this study, we compared the permeabilization effects of LL-37, melittin, and alamethicin, using two dye molecules of different sizes. We quantify the permeabilization of lipid bilayers and cell membranes by each AMP with respect to a chosen dye molecule. It is known that cell death also induces membrane permeabilization, so we also compared the effect of AMPs with the effects of metabolic inhibitor carbonyl cyanide *m*-chlorophenylhydrazone (CCCP) and daptomycin. The results show that AMPs induce a unique pattern of intracellular fluorescence intensity time curve. The patterns and the membrane permeability induced in spheroplast and in GUVs reveal the similarities and dissimilarities between cell membranes and model lipid bilayers as well as the characteristics of different AMPs. Overall, the lipid bilayers remarkably reproduced the main features of the AMPs' action on cell membranes.

MATERIALS AND METHODS

Bacterial strains and culture conditions

E. coli K-12 strain MG1655 (ATCC 700926) was purchased from American Type Culture Collection (Manassas, VA). Luria-Bertani medium (EMD, 5 g/L yeast extract, 10 g/L peptone from casein, and 10 g/L sodium chloride) containing 15 g/L agar (EMD) was used for *E. coli* growth at 37°C with shaking.

Chemicals

Sucrose, glucose, tris, hydrochloric acid, sodium hydroxide, lysozyme, DNase, EDTA, magnesium chloride, carbonyl cyanide 3-chlorophenylhydrazone (CCCP), cephalexin, melittin, and alamethicin were purchased from Sigma Aldrich (St. Louis, MO). Daptomycin was purchased from Selleckchem (Houston, TX). 1-palmitoyl-2-oleoyl-*sn*-glycero-3-phosphocholine (POPC), 1,2-dioleoyl-*sn*-glycero-3-phosphocholine (DOPC), 1,2-dioleoyl-*sn*-glycero-3-phospho-(1′-rac-glycerol) (DOPG), 1,2-dioleoyl-*sn*-glycero-3-phosphoethanolamine-*N*-cap biotinyl (biotin-DOPE), and 1,2-dioleoyl-*sn*-glycero-3-phosphoethanolamine-*N*-lissamine rhodamine B sulfonyl (Rh-DOPE) were purchased from Avanti Polar Lipids (Alabaster, AL). Calcein, FITC dextran 4000, and sytox orange (SO) were purchased from Invitrogen (Grand Island, NY). LL-37 was produced by GenScript (Piscataway, NJ). Polydimethylsiloxane (PDMS; Dow Corning Sylgard 184) was purchased from Electron Microscopy Sciences (Hatfield, PA).

Perfusion chamber

Silicone sheets (McMaster Carr, Elmhurst, IL) were laser cut to 24 × 27 mm rectangles with a diamond or channel in the center (Fig. S1). The silicone sheet was pressure sealed to a 24 × 50 mm coverslip. A slab of PDMS was punched with 23-gauge dispensing needles (McMaster Carr) bent 90°. The PDMS slab was pressure fit onto the silicone sheet to seal the chamber. Tubing connected the dispensing needles to open syringes fitted with two-way stopcocks. Solutions from the syringes entered the perfusion chamber by gravity and flowed into a waste container.

Spheroplast production and experimental setup

E. coli giant spheroplasts were prepared as described in the literature (15–17). Briefly, cells were grown in Luria-Bertani medium and cephalexin was added to inhibit cell division. Filamentous cells with an average length of 50 μm were harvested and incubated with lysozyme to remove the cell wall and outer membrane. STOP solution (10 mM Tris-HCl, pH 8.0, 0.7 M sucrose, 20 mM $MgCl_2$) was added to stabilize the spheroplasts. Spheroplasts were stored in liquid nitrogen or −80°C and thawed on ice before use.

Perfusion chambers were coated with 0.01% poly-L-lysine and left overnight, then washed with distilled water and air dried. Spheroplasts were injected into a perfusion chamber and incubated for at least 1 h. The experiment started with a STOP solution containing 40 μM calcein perfused for 5 min. AMP was prepared in STOP solution with 40 μM calcein and perfused for the next 5 min. Flow was then stopped. The AMP concentrations are: melittin 0.5–5.0 μM, LL-37 1 μM, alamethicin 2 μM, CCCP 100 μM, daptomycin 1 μM with 1 mM $CaCl_2$.

GUV production and experimental setup

GUVs were prepared by electroformation (18) as described in Sun et al. (19). To represent model membrane studies, we arbitrarily chose the lipid POPC, one of the often used lipids in such studies. For AMP experiments, the lipid mixture was POPC/biotin-DOPE/Rh-DOPE (98:1:1 mol %). For daptomycin experiments, the lipid mixture contained DOPC/DOPG/biotin-DOPE/Rh-DOPE (68:30:1:1 mol %); the reason is that daptomycin targets only phosphatidylglycerol (PG)-containing membranes (20). The lipid mixes were dissolved in chloroform/trifluoroethanol (1:1) to a final concentration of 1 mM. A quantity of 40 nmol of lipid was spread onto each of two clean 25 × 25 mm indium tin oxide-coated glass slides (Structure Probe, West Chester, PA) and air dried. Residual solvent was removed under vacuum for 60 min. A rubber O-ring was used to form a chamber to hold a 200 mM sucrose solution. A function generator was used to apply a 10 Hz sine wave at 3.5 Vptp to the chamber for 2 h. The frequency was reduced to 5 Hz for 10 min followed by 1 Hz for 10 min. GUVs were harvested and used within 48 h.

Perfusion chambers were coated with biotin-BSA (5 mg/mL) for 1 h and washed with distilled water. The chamber was then coated with avidin (0.5 mg/mL) for 2 h. GUVs were diluted with 200 mM glucose, injected into the perfusion chamber, and incubated for 1 h. Control solution, containing 200 mM glucose and 40 μM calcein, was perfused into the chamber for 5 min. A second solution, containing 200 mM glucose, 40 μM calcein, and an AMP or another chemical agent, was perfused for 5 min and then

flow was stopped. The AMP concentrations are: melittin 2.0 μM, alamethicin 0.5 μM, daptomycin 1 μM with 1 mM $CaCl_2$.

Laser scanning confocal microscopy

Laser scanning confocal time series were collected on an Eclipse Ti microscope (Nikon, Melville, NY) equipped with a 100× Plan Fluor objective (Nikon). Calcein and FITC were excited with a 488 nm laser (Coherent, Bloomfield, CT) and 573–613 nm excitation light was captured. Rhodamine and SO were excited with a 561-nm laser (Coherent) and 650–1000 nm excitation light was captured. Time intervals between image acquisitions was 60 s except for photobleach periods where the interval was 5 s. Photobleaching was conducted only after the intracellular fluorescence reached steady state. The intracellular (intravesicular) fluorescence intensities shown in the figures were normalized as follows, where the subscripts "in" and "out" represent intracellular (intravesicular) and extracellular (extravesicular), respectively:

$$\text{Normalized intracellular fluorescence} = \frac{F_{\text{in}(t)} - F_{\text{out}(t)} \times \dfrac{F_{\text{in}(o)}}{F_{\text{out}(0)}}}{F_{\text{out}(t)} - F_{\text{out}(t)} \times \dfrac{F_{\text{in}(o)}}{F_{\text{out}(0)}}}.$$

The extracellular (extravesicular) fluorescence intensity shown in the figures is the denominator normalized to its initial value at $t = 0$.

Data analysis

Images were processed in the software Fiji (https://fiji.sc) (21) using custom macros. Data were further processed and graphed using custom Python scripts (https://www.python.org/), which relied on the NumPy (http://www.numpy.org/), Pandas (http://pandas.pydata.org/), Matplotlib (http://matplotlib.org/), SciPy (https://www.scipy.org), and pybeeswarm packages (https://pypi.python.org/pypi/pybeeswarm). FreeCAD (https://www.freecadweb.org/) was used to draw the perfusion chamber diagram (Fig. S1 in the Supporting Information). Figures were assembled in Inkscape (https://inkscape.org/en/).

RESULTS

A perfusion chamber was designed to allow precise control over the timing and concentration of AMPs delivered to immobilized spheroplasts or GUVs (Fig. S1). In the chamber, spheroplasts were immobilized by adhering to a coverslip coated with poly-L-lysine (22) or GUVs containing 0.5 mol % biotinylated lipid adhered to a surface coated with avidin. A representative experiment observing the leak-in of calcein through the melittin-induced permeability in *E. coli* spheroplasts is shown in Fig. 1 *a*. The spheroplasts were first stabilized in a solution containing 40 μM calcein for 5 min. The same solution containing 1.0 μM melittin was introduced into the chamber and perfused for 5 min, then the flow was stopped. We have tested and found that the solution in the chamber is completely replaced by 5 min perfusion (Fig. S1).

No calcein leakage into the spheroplast was observed during the initial 5 min control period before the introduction of AMPs. After melittin was added, no leakage was observed for ~10 min. Calcein then leaked into the spheroplast and the intracellular fluorescence intensity rose to a steady-state level. The steady-state level of intracellular fluorescence intensity was always less than (~0.8 times) the extracellular intensity level. The rise to steady state was captured using a 60-s interval between image acquisitions, which amounted to little photobleaching. The interval between image acquisitions was then shortened to 5 s and an exponential decay of the intracellular intensity was observed—we call this a "photobleaching" period. After the photobleaching period, the image acquisition interval was increased back to 60 s and the intracellular fluorescence intensity recovered to the previous steady state. The 5-s photobleaching was repeated at least once during each experiment to make sure that the steady-state levels and exponential decays were internally consistent. Note that photobleaching is absent for the extracellular fluorescence intensity because the dye molecules outside the cell mixed rapidly with unbleached dye molecules beyond the lighted region. If the exchange of dye molecules between inside and outside of the cell were free diffusion, there would be no photobleaching effect for the intracellular fluorescence intensity. The image of the cell was recorded during the entire process to see if there was any morphological change (Movie S1).

Compared with our previous measurements on *E. coli* spheroplasts in Sun et al. (15), this experiment was considerably simplified because we intended to repeat the same experiment with both spheroplasts and GUVs, with several different peptides and dye molecules. Because of the stochastic nature of peptide-membrane interactions (8,11,23,24), each measurement was repeated many times to examine its reproducibility. From each intracellular fluorescence intensity time curve we parameterize the following characteristics: the lag time from the introduction of AMP to the beginning of leakage, the rise time from the beginning of leakage to the time reaching the steady state, and the flux rate of dye during the steady state that represents the membrane permeability induced by the peptide. The regularity of

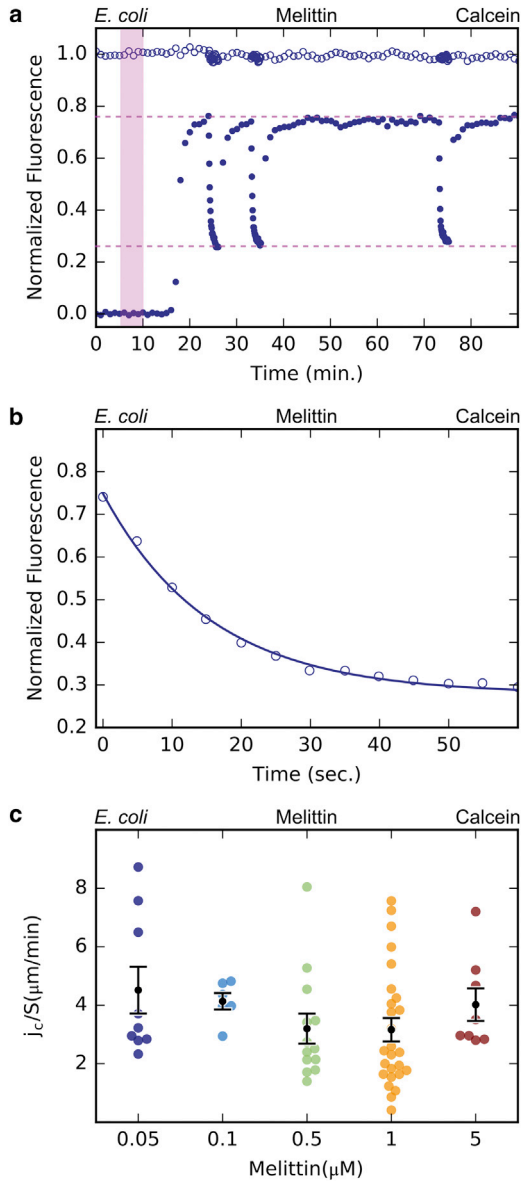

FIGURE 1 Membrane permeability induced by melittin in *E. coli* spheroplasts. (*a*) A confocal time series of immobilized *E. coli* spheroplasts in a perfusion chamber was collected. Solution containing calcein, but no melittin was perfused from 0-5 min followed by perfusion of calcein with melittin (1 μM) from 5–10 min (*shaded pink region*). Perfusion was then stopped at 10 min. Normalized extracellular (*open circles*) and intracellular (*filled circles*) calcein fluorescence intensities are shown. The interval between scans was 60 s, except for the photobleaching periods where the interval was 5 s. The upper pink dashed line is the steady state level of intracellular fluorescence intensity with negligible photobleaching when the scan interval was 60 s (C_{s1}). The lower pink dashed line is the steady state level of intracellular fluorescence intensity during photobleaching when the scan interval was 5 s (C_{s2}). (*b*) Exponential curve fitting of the calcein fluorescence during photobleaching was used to find the decay constant τ_e and calculate total flux rate through the membrane (see text for full description). (*c*) Normalized calcein flux rate, j_c divided by the membrane area (j_c/S), over a range of melittin concentrations (0.05 – 5 μM) is shown. Each colored dot represents the normalized flux rate during one photobleaching measurement. Black dots represent the mean flux rate per unit area at one melittin concentration and the error bars are the standard error of the mean (SEM). There is no correlation between melittin concentration and flux rate.

the fluorescence intensity curves and cell morphology are also noted.

We used a simple model to analyze the intracellular fluorescence time curve (15). Let $C(t)$ be the unbleached calcein concentration inside the spheroplast at time t, and C_{out} be the extracellular concentration of unbleached calcein. Its kinetics can be described by the equation:

$$\frac{dC(t)}{dt} = -\frac{1}{\tau}C(t) - \frac{j_c}{V}C(t) + \frac{j_c}{V}C_{\text{out}}. \qquad (1)$$

On the right-hand side of the equation, the first term is the reduction rate due to photobleaching with a rate constant τ that depends on the intensity of the illumination. The second term is the total efflux j_cC divided by the cell volume V, and the third term is the total influx j_cC_{out} divided by V. As introduced in the previous article (15), j_c represents the permeability of the membrane. The value j_c multiplied by the molecular concentration on one side of the membrane is the total flux (number of molecule per second) diffusing through the membrane to the other side. If the permeability is due to a circular pore of radius a in a membrane of negligible thickness, then $j_c = 4aD$, where D is the diffusion constant of the molecule (25). The unit of flux rate j_c is volume per second. Because j_c is proportional to the membrane area (Fig. S2), for comparison we normalize it to per unit area of membrane.

When the membrane permeability is a constant, the intracellular fluorescence intensity should reach a steady state under a given photobleaching rate $1/\tau$, namely, $dC(t)/dt = 0$, $C(t) \to C_s$. The flux rate j_c is a constant that satisfies the relation $C_s/\tau_e = j_cC_{\text{out}}/V$, with $1/\tau_e = 1/\tau + j_c/V$ (see (15)). Fig. 1 *a* shows two steady states, one with little photobleaching (with 60-s interval image taking) during which $C(t) \to C_{s1}$ at the top level, and another with 5-s interval photobleaching during which $C(t) \to C_{s2}$. The decay from C_{s1} to C_{s2} follows the relation $C(t) - C_{s2} = (C_{s1} - C_{s2})e^{-t/\tau_e}$ (Fig. 1 *b*). Thus we can use the measured decay constant τ_e (Fig. 1 *b*) and the ratio C_{s2}/C_{out} to obtain the flux rate $j_c = C_{s2}V/C_{\text{out}}\tau_e$ (see details in (15) including a correction for the intracellular volume accessible to the dye molecules). The same experiment was repeated at five different melittin concentrations from 0.05 to 5.0 μM (Fig. 1 *c*).

E. coli spheroplasts reacted to LL37 and alamethicin similarly to melittin (Fig. 2, *a* and *b*). Using the dye-molecule FITC dextran 4000 (six times larger than calcein) did not change the pattern of the intracellular fluorescence intensity curve, but the flux rate was decreased (Fig. 2 *c*) as expected, due to a smaller diffusion constant (Stokes-Einstein law) and possibly a greater friction through a finite-sized pore for a larger molecule. The upper steady-state level of the (normalized) FITC intracellular fluorescence intensity is higher than that of calcein. The physical basis for the upper limit of the internal fluorescence intensity is unknown. We imagine that the intracellular molecules spatially exclude the dye

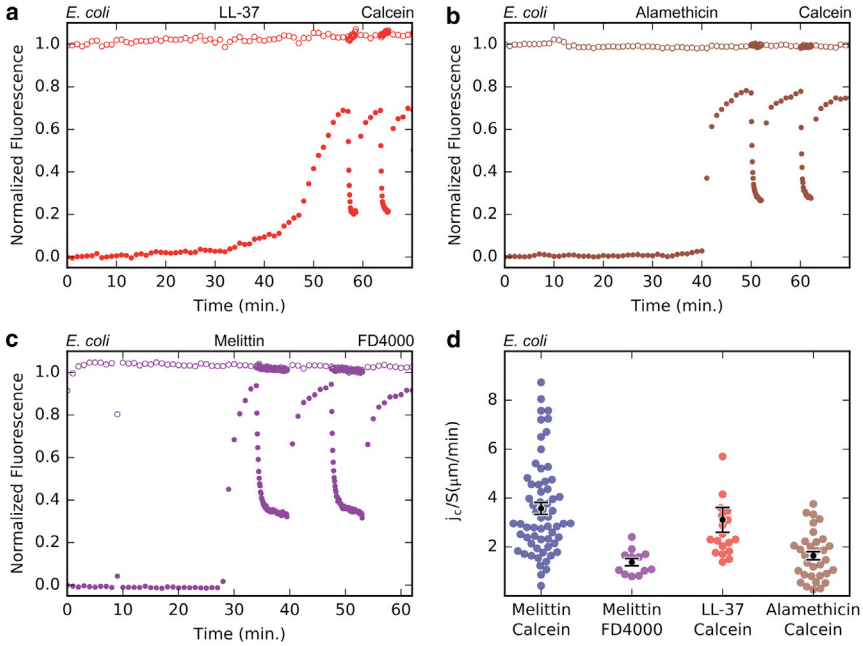

FIGURE 2 Membrane permeability induced by AMPs in *E.coli* spheroplasts. Experiments were conducted as described in Fig. 1 a, but with different peptides or fluorescent dye. (*a*) Calcein permeability induced by LL-37 (1 μM) and (*b*) by alamethicin (2 μM). (*c*) FITC-dextran 4000 (FD4000) permeability induced by melittin (1 μM). (*d*) Summary of normalized flux rate through *E. coli* membranes. Each colored dot represents the value of j_c/S by one photobleaching measurement. The black dots represent the mean normalized flux rate and the error bars are the SEM. The data for calcein flux rate induced by melittin are shown in an aggregated form taken from Fig. 1 *c*.

molecules, thus reducing the averaged dye concentration (15); but they might bind the dye molecules, and this would have the opposite effect. Membrane permeability is only calculated from the exponential decay during photobleaching. It should be independent of this upper limit.

The flux rates per unit area from a large number of repeated measurements were averaged (Fig. 2 *d*). The rates are practically the same for melittin and LL37; ~50% smaller for alamethicin.

We compared the membrane permeabilization induced by AMPs with the permeabilization caused by poison CCCP. Spheroplasts were exposed to CCCP in the presence of calcein and SO. SO fluoresces when bound to DNA and should not cross the membrane of live cells. Both fluorescent dyes slowly leaked into the cell after the CCCP exposure (Fig. 3 *a*; Fig. S3; Movie S2). The initial leakage of calcein is much slower than AMP treatment. The initial leakage of SO is similar to calcein but, after a certain point, the sytox fluorescence begins to decline. This decrease could be due to the loss of DNA as the membrane loses integrity.

Daptomycin is an FDA-approved antibiotic against Gram-positive pathogens (20,26). It acts with calcium ions targeting bacterial membranes containing PG (27) and kills cells by inducing membrane permeability to potassium ions (20,26). Because *E. coli* cytoplasmic membrane contains a substantial amount of PG (28,29), we suspect that daptomycin might be active against *E. coli* spheroplasts (without the possible protection by the outer membrane). Indeed we found that the effect of daptomycin to spheroplast is similar to CCCP (Fig. 3 *b*; Fig. S3; Movie S3). On the other hand, daptomycin does not induce permeability to calcein in a PG-containing GUV (made of DOPC/DOPG 7:3; see Movie S4). Instead, it showed a lipid-extracting effect, where daptomycin induces lipid aggregates that appear to emerge from the membrane (Movie S4), in agreement with a previous report (30).

For comparison with a model lipid bilayer, we chose a commonly used lipid, POPC. GUVs of POPC/biotin-DOPE/Rh-DOPE (99.5:0.5:1 mol %) were produced encapsulating 200 mM sucrose and immersed in 200 mM glucose. The biotin-DOPE was for immobilizing the GUVs in the flow

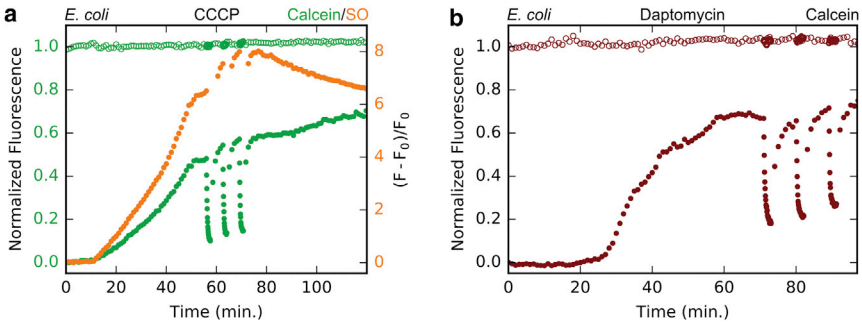

FIGURE 3 Membrane permeability induced by CCCP and daptomycin in *E. coli* spheroplasts. Experiments were conducted as described in Fig. 1 *a*, but with different chemicals or fluorescent dyes. (*a*) Calcein and sytox orange (SO) permeability induced by CCCP (100 μM) in *E. coli* membranes is shown. The SO signal is represented as an increase from the initial state, $(F-F_0)/F_0$. (*b*) Calcein permeability induced by 1 μM daptomycin with 1 mM $CaCl_2$.

chamber. The Rh-DOPE was for viewing the GUV membranes. The sucrose and glucose were used to control the osmolality and provide a phase contrast (31). The response of GUVs to the attack of melittin was surprisingly similar to spheroplasts (Fig. 4 *a*; Movie S5). As soon as the dye molecules leaked into the GUV, its phase contrast was lost, indicating mixing of intra-GUV sucrose with extra-GUV glucose. Alamethicin-induced permeability in GUVs (Fig. 4 *b*) is qualitatively similar to melittin (Fig. 4 *a*); however, calcein flux rate is lower for alamethicin than melittin (Fig. 4 *c*). This behavior matches that seen in *E. coli* spheroplasts. Repeated measurements showed that, statistically, lag and rise times in GUVs are shorter than in spheroplasts (Fig. 4, *d–f*). But, importantly, the average steady-state permeability induced in GUVs is in agreement with the average steady-state permeability induced in spheroplasts (Fig. 4 *c*). The summary of all measurements is listed in Table S1.

There are, however, differences between spheroplast and GUV. Whereas spheroplasts are apparently insensitive to the AMP concentration, at least from 0.05 to 5 μM, GUVs are very sensitive to the AMP concentration. Fig. 4 *a* and repeated measurements were performed with 2 μM melittin. Attempts to measure GUVs at 5 μM melittin resulted in vesicle rupture. At concentrations <2 μM melittin, the response of GUV was inconsistent, sometimes behaving like 2 μM melittin (Fig. 4 *a*), and sometimes with no response for a long time.

DISCUSSION

Since the discovery of host defense AMPs in the early 1980s, there has been continuous interest in their molecular mechanisms, in part due to the desire to select or synthesize ideal AMPs for therapeutic uses (4,7,32–34). Initially there were questions about the molecular targets of these antimicrobials. By the late 1980s, accumulated evidence, especially the experimental results that the natural all-L peptides and their D enantiomers were equally active (34), convincingly concluded that the main targets of AMPs were the bacterial cytoplasmic membranes, rather than stereospecific molecular receptors (4). But how to determine the molecular mechanism against bacterial membranes has been an open question. There are microscopy observations of dye-labeled AMPs attacking live bacteria (7–11,35) that show the cytoplasmic membranes being permeabilized, allowing the AMPs to enter the cell. Another study estimated the amount of a dye-labeled AMP accumulated on bacterial membranes at the condition of bactericidal assay (36). But the membrane permeabilization has neither been characterized nor quantified.

In our previous study (15) we showed a method of measuring instantaneous permeability j_c through the bacterial membrane of a spheroplast. This quantity j_c, in the unit of volume per second, represents the membrane permeability to a dye molecule, independent of its concentration. In this article, we introduced a flow chamber in which spheroplasts or GUVs are exposed to a solution of AMP and dye molecules under time control. The time-dependent permeability through the membrane is reflected by the intracellular fluorescence intensity of the dye molecules (as shown in (15)). Thus we characterize the permeabilization of the spheroplast or GUV membrane by the time-dependent pattern of the intracellular fluorescence intensity, including a quantitative measure of the permeability j_c when the latter

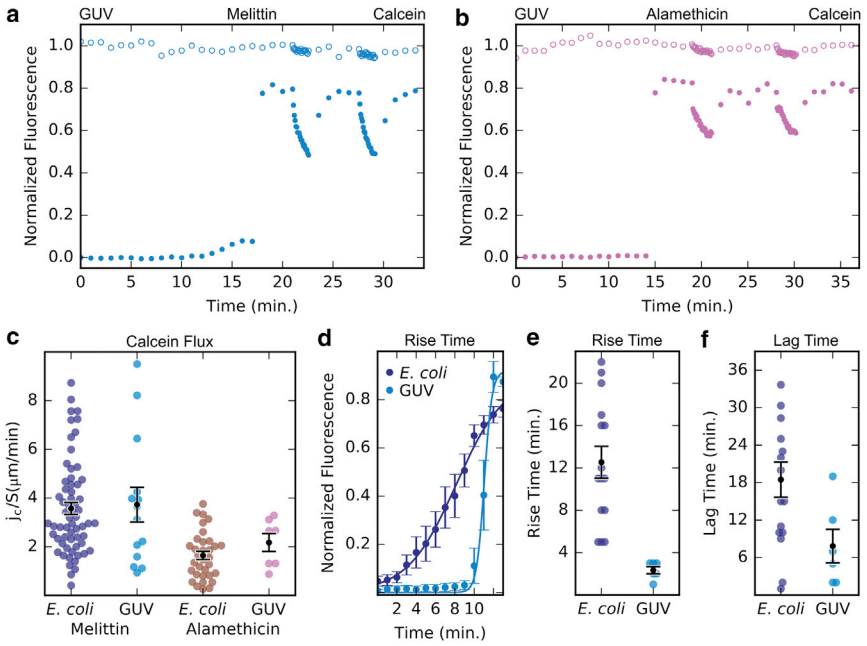

FIGURE 4 Comparison of AMP-induced membrane permeability in *E. coli* and GUVs. (*a* and *b*) Experiments were conducted as described in Fig. 1 *a*, but with POPC:biotin:DOPE:Rh-DOPE GUVs (98:1:1 mol%) immobilized on a avidin-coated surface, using melittin (2 μM) and alamethicin (0.5 μM), respectively. (*c*) Normalized calcein flux rate (j_c/S) in *E. coli* and GUV membranes induced by melittin and alamethicin are compared. (The *E. coli* data were previously shown in Fig. 2 *d*.) (*d* and *e*) The rise time between the onset of calcein influx and the time reaching the steady state is shorter for GUVs than *E. coli*. (*d*) shows the average of the rise from baseline to steady state for *E.* coli (average of 10 runs) and GUVs (average of 6). Dots are the average calcein intensity and the line was curve fitting. Error bars = SEM. (*e*) All rise times for *E. coli* and GUVs are compared. Colored dots represent individual measurements and black dots the average. Error bars = SEM. (*f*) The lag time, the time between the start of melittin addition (the 5th min) and when calcein leakage begins, is shorter for GUVs than *E. coli*. Melittin may take longer to attack *E. coli* due to the complexity of the membrane.

reaches a steady state. Because j_c is proportional to the membrane area (Fig. S2), for comparison we normalize it to per unit area of membrane, j_c/S. There are variations in the lag time after AMP was brought in and before leakage began. The rise time from the onset of leakage to the time reaching a steady state also varies. Such stochasticity is in general consistent with observations in live cell experiments (8,11). Accordingly, each measurement was repeated a large number of times for obtaining meaningful statistical averages.

We tested three AMPs: Bee venom toxin melittin (37), which is perhaps the most extensively studied antimicrobial (38–42); human AMP LL37 (43); and alamethicin, which is the only member of AMPs that has been shown to form barrel-stave pores (44,45) in lipid bilayers. Other members of AMPs that have been studied, including melittin and LL37, form toroidal pores (41,46,47) in lipid bilayers.

The action of AMPs on spheroplast has a well-defined pattern

It is well known that metabolic inhibitor CCCP dissipates the proton gradient across the cell membrane, leading to cell death and loss of membrane integrity (48–50). Figs. 3 *a* and S2 show seven separate runs of spheroplasts poisoned by CCCP. In all cases, the leak-in of calcein always started near the end of the 5 min period during which the sample chamber was perfused with the solution containing CCCP. This indicates a very definitive action of CCCP. However, the time patterns of the intracellular fluorescence intensity are irregular: the increase was slow (compared with the action of AMPs) and not smooth, including sudden increases and decreases. One might describe the patterns as due to irregular membrane defects slowly accumulated in the membrane. The permeability did not rise to a steady-state value. The movies of the image show sudden changes of the cell volume (Movie S2). The patterns due to daptomycin are somewhat similar (Fig. 3 *b*). Daptomycin causes cell death by inducing membrane permeability to atomic ions. Its effect on lipid bilayers does not cause leakage to calcein (Movie S4). The primary actions of CCCP and daptomycin on spheroplasts are proton and potassium ion leakage, respectively, which cause the cell death. The membrane permeability to calcein was the secondary effect in both cases.

In contrast, the intracellular fluorescence intensity patterns of a spheroplast attacked by AMPs follow a regular pattern (Figs. 1 *a* and 2, *a–c*). There is always a lag time before the calcein leak-in. Then the fluorescence intensity always rises in a smooth sigmoidal fashion to a steady state. The regular patterns include a common average steady-state membrane permeability independent of AMP concentrations, at least from 0.05 to 5.0 μM (Fig. 1 *c*). The cell boundaries of spheroplasts under AMP attack were always stationary, exhibiting little change (Movie S1). Note that in our previous study (15), melittin was released from a pipe by diffusion, thus the delivery time of AMPs was not well defined. As a result, there were greater variations in the sigmoidal rise time. The AMP concentration in this study was under much better control, which produced more regular intensity patterns. This implies that AMPs induce membrane permeability with a well-defined, reproducible mechanism.

The actions of AMPs on GUVs and on *E. coli* spheroplasts are remarkably similar

Cell membranes differ from a simple lipid bilayer at least in their lipid composition complexity, leaflet asymmetry, protein content, and possible lipid domains. In an earlier study on *E. coli* spheroplast membranes (17), we found that stretching (i.e., area increase by an applied tension) of the cytoplasmic membranes is reversible, but the elastic coefficient is one order-of-magnitude smaller than that of stretching a lipid bilayer (17). We believe that this is due to the existence of a membrane reservoir. And, perhaps for that reason, cytoplasmic membranes of *E. coli* spheroplasts maintain a tensionless condition over a wide range of external osmolality (17). Given such differences between spheroplast membranes and model lipid bilayers, one might expect different responses to the attack of AMPs. Surprisingly, what occurred in GUVs is very similar to what occurred in spheroplasts. Firstly, AMPs induced an intravesicular fluorescence intensity pattern (Fig. 4, *a* and *b*) very similar to that induced in spheroplasts (Figs. 1 *a* and 2, *a–c*). Secondly, the steady-state permeability per unit area values induced in spheroplasts and GUVs are in good agreement despite the size variations (Fig. 4 *c*; Table S1).

However, there are interesting differences in details between GUVs and spheroplasts. First, the rise time from the beginning of leakage to the steady state is much shorter in GUVs than in spheroplasts (Fig. 4, *d* and *e*). Second, the image of a GUV under attack initially appeared to be a tense sphere, but once the intravesicle fluorescence reached the steady state, the GUV membrane began to undulate (Movie S5); in comparison, the image of a spheroplast under AMP attack appeared to be unchanging with time (Movie S1). Third, spheroplasts reached practically the same steady-state membrane permeability independent of AMP concentration from 0.05 to 5.0 μM. In contrast, GUVs reached a steady state only at a chosen AMP concentration (Fig. 4). When we tried to vary the AMP concentrations as we did for spheroplasts, we found that at higher AMP concentrations, GUVs ruptured easily; at lower AMP concentrations, the leakage was too slow to perform the experiment. Perhaps the difference in sensitivity to AMP concentration is in part due to the bacterial membranes being negatively charged (28,29) whereas our GUVs are made of neutral POPC. Another reason for the

differences between spheroplasts and GUVs could be the membrane tension—see below.

Understanding the action of AMPs

Many investigators of AMPs have proposed different ways of explaining how AMPs induce membrane permeabilization, such as the carpet model (51), detergentlike action (52), the interfacial activity model (53), and variations of these models (54,55)—or a suggestion that there are no definitive mechanisms among AMPs (55). All models of membrane permeabilization are of course consistent with the dye leakage through the membranes. However, none of the above-mentioned models is, as far as we know, specific enough for us to compare with the time pattern of the leakage phenomena shown in our results.

That AMPs induce transmembrane pores in lipid bilayers is well supported by phenomenological analyses (46,54,56) as well as by direct structural evidence from neutron in-plane scattering (44,47,57) and x-ray diffraction (45,46,58). AMPs are amphipathic peptides. Almost all measurements agree (59–63) that helical peptides initially bind on the bilayer's hydrophilic-hydrophobic interface parallel to the plane of the bilayer. In this condition, the membrane area expands in proportion to the bound peptide-to-lipid ratio (P/L), otherwise the bilayer exhibits no permeability (46). Also, in this condition, no peptide aggregates were detected (62,64,65), particularly by fluorescence energy transfer (66). But when P/L exceeds a critical value P/L*, the lipid bilayer loaded with peptides in high P/L transforms to a new state with pores that are stabilized by a peptide distribution both on the interface and on the luminal surface of the pores (46,67). The time dependence of the fluorescence intensity patterns observed in spheroplast are consistent with this two-state transition (68). The initial peptide binding with P/L still below P/L* gives rise to a lag time. The leakage begins only when P/L exceeds P/L*, and the membrane settles into a steady state of constant permeability. The steady state implies that there is a free-energy minimum state at a certain pore concentration in the membrane, surprisingly independent of the AMP concentration (at least from 0.05 to 5.0 μM).

One difference between GUVs and spheroplasts is that GUVs are often produced with a surface tension whereas spheroplast membranes have been found to be tensionless (17). The pore size would expand by a membrane tension, as expected from the membrane mechanics (69–71). A GUV with a membrane tension must have an internal pressure higher than outside (according to the Laplace equation (72)). But once pores open in the membrane both the pressure differential and tension will diminish, and the pore size will also decrease accordingly. Thus, compared with spheroplasts, the initial pores formed in GUVs are larger, which explains the shorter rising time (Fig. 4, *d* and *e*). Independently, there are previous studies (23,24) reporting that AMP induced pores in GUVs initially allowing the passage of dye molecules of ~10 kDa, but in later time allowing only smaller dye molecules. Another consequence of GUV losing tension is the visible undulations of tensionless membranes in GUVs (73,74) as seen in Movie S5. Spheroplast membranes appeared to be stationary, clearly different from a lipid bilayer (Movie S1).

Perhaps the bacterial membrane consists of small lipid domains as recently suggested (75), making it more stable than a GUV, which consists of one large lipid domain. Spheroplast membranes with a steady-state permeability are stable for at least an hour, whereas GUV membranes with pores strongly undulate and often rupture, particularly in high concentrations of AMPs. Only in the bacterial membranes could one have discovered the existence of a steady state of AMP-induced permeability over a wide range of AMP concentrations. It is impossible to perform GUV experiment with high concentrations of AMPs due to the fragility of pure lipid bilayers.

Alamethicin forms barrel-stave pores (44,45); melittin and LL37 form toroidal pores (41,46,47). Despite these differences, the time-dependent intracellular fluorescence patterns in spheroplasts induced by three different AMPs are very similar in lag and rise times. The calcein flux rates per unit area j_c/S by alamethicin and melittin are, respectively, 1.6 $\pm$ 0.2 and 3.6 $\pm$ 0.3 μm/min in spheroplasts and 2.2 $\pm$ 0.4 and 3.7 $\pm$ 0.7 μm/min in GUVs. The actions of LL37 and melittin are similar both qualitatively and quantitatively. The flux rate differences between alamethicin and melittin can be understood by the different dimensions for the two types of pores. The interior diameter of alamethicin pores is 1.8 nm (76), whereas melittin and LL-37 pores are ~4.4 nm (41,47), as measured by in-plane neutron diffraction. All of these characteristics measured in lipid bilayers were faithfully reproduced in spheroplasts. Thus both barrel-stave and toroidal pore-forming AMPs follow the same two-state mechanism (68).

CONCLUSIONS

The most surprising and important result is that the action of AMPs on GUVs is closely similar to the action on *E. coli* spheroplasts. Under the tensionless condition, the steady-state permeabilities per unit area induced by AMPs in spheroplast cytoplasmic membranes and in GUV lipid bilayers are in good agreement for the melittin and alamethicin tested here. Thus, most likely AMPs induce pore formation in the bacterial membranes just as they do in model lipid bilayers. When we used FITC dextran 4000 in place of calcein with melittin-attacking spheroplasts (Fig. 2 *c*), the flux rate was reduced from 3.6 $\pm$ 0.3 μm/min to 1.4 $\pm$ 0.2 μm/min (Fig. 2 *d*), consistent with the permeability being caused by transmembrane pores of a finite size. Besides the understandable differences between spheroplasts and GUVs discussed above,

our results strongly support the validity of model membranes studies of AMPs. Although we have shown some aspects of spheroplast experiment that are probably difficult to reproduce by GUVs, clearly experiments with live cells are more limited than with lipid bilayers. We have to rely on model membrane studies to understand the molecular interactions.

SUPPORTING MATERIAL

Three figures, one table, and five movies are available at http://www.biophysj.org/biophysj/supplemental/S0006-3495(17)30289-8.

AUTHOR CONTRIBUTIONS

J.E.F. and H.W.H. designed the research. J.E.F. and P.-Y.Y. performed the experiments. J.E.F. and P.-Y.Y. analyzed the data. J.E.F. and H.W.H. wrote the article.

ACKNOWLEDGMENTS

This work was supported by NIH grant No. GM55203 and Robert A. Welch Foundation grant No. C-0991.

REFERENCES

1. Gorter, E., and F. Grendel. 1925. On bimolecular layers of lipoids on the chromocytes of the blood. *J. Exp. Med.* 41:439–443.
2. Danielli, J. F., and H. Davson. 1935. A contribution to the theory of permeability of thin films. *J. Cell. Comp. Physiol.* 5:495–508.
3. Mueller, P., D. O. Rudin, …, W. C. Wescott. 1962. Reconstitution of cell membrane structure in vitro and its transformation into an excitable system. *Nature.* 194:979–980.
4. Boman, H. G., J. Marsh, and J. A. Goode, editors 1994. Antimicrobial Peptides. John Wiley and Sons, Chichester, UK.
5. Cottagnoud, P. 2008. Daptomycin: a new treatment for insidious infections due to Gram-positive pathogens. *Swiss Med. Wkly.* 138:93–99.
6. Cass, A., A. Finkelstein, and V. Krespi. 1970. The ion permeability induced in thin lipid membranes by the polyene antibiotics nystatin and amphotericin B. *J. Gen. Physiol.* 56:100–124.
7. Steiner, H., D. Andreu, and R. B. Merrifield. 1988. Binding and action of cecropin and cecropin analogues: antibacterial peptides from insects. *Biochim. Biophys. Acta.* 939:260–266.
8. Sochacki, K. A., K. J. Barns, …, J. C. Weisshaar. 2011. Real-time attack on single *Escherichia coli* cells by the human antimicrobial peptide LL-37. *Proc. Natl. Acad. Sci. USA.* 108:E77–E81.
9. Rangarajan, N., S. Bakshi, and J. C. Weisshaar. 2013. Localized permeabilization of *E. coli* membranes by the antimicrobial peptide Cecropin A. *Biochemistry.* 52:6584–6594.
10. Barns, K. J., and J. C. Weisshaar. 2013. Real-time attack of LL-37 on single *Bacillus subtilis* cells. *Biochim. Biophys. Acta.* 1828:1511–1520.
11. Fantner, G. E., R. J. Barbero, …, A. M. Belcher. 2010. Kinetics of antimicrobial peptide activity measured on individual bacterial cells using high-speed atomic force microscopy. *Nat. Nanotechnol.* 5:280–285.
12. Seigneuret, M., and P. F. Devaux. 1984. ATP-dependent asymmetric distribution of spin-labeled phospholipids in the erythrocyte membrane: relation to shape changes. *Proc. Natl. Acad. Sci. USA.* 81:3751–3755.
13. Martin, O. C., and R. E. Pagano. 1987. Transbilayer movement of fluorescent analogs of phosphatidylserine and phosphatidylethanolamine at the plasma membrane of cultured cells. Evidence for a protein-mediated and ATP-dependent process(es). *J. Biol. Chem.* 262:5890–5898.
14. Rodriguez, N., J. Heuvingh, …, S. Cribier. 2005. Indirect evidence of submicroscopic pores in giant unilamellar vesicles. *Biochim. Biophys. Acta.* 1724:281–287.
15. Sun, Y., T. L. Sun, and H. W. Huang. 2016. Mode of action of antimicrobial peptides on *E. coli* spheroplasts. *Biophys. J.* 111:132–139.
16. Renner, L. D., and D. B. Weibel. 2011. Cardiolipin microdomains localize to negatively curved regions of *Escherichia coli* membranes. *Proc. Natl. Acad. Sci. USA.* 108:6264–6269.
17. Sun, Y., T. L. Sun, and H. W. Huang. 2014. Physical properties of *Escherichia coli* spheroplast membranes. *Biophys. J.* 107:2082–2090.
18. Angelova, M. I. 2000. Liposome electroformation. *In* Giant Vesicles. P. L. Luisi and P. Walde, editors. John Wiley, Chichester, UK, pp. 27–36.
19. Sun, Y., W. C. Hung, …, H. W. Huang. 2009. Interaction of tea catechin (−)-epigallocatechin gallate with lipid bilayers. *Biophys. J.* 96:1026–1035.
20. Silverman, J. A., N. G. Perlmutter, and H. M. Shapiro. 2003. Correlation of daptomycin bactericidal activity and membrane depolarization in *Staphylococcus aureus*. *Antimicrob. Agents Chemother.* 47:2538–2544.
21. Schindelin, J., I. Arganda-Carreras, …, A. Cardona. 2012. Fiji: an open-source platform for biological-image analysis. *Nat. Methods.* 9:676–682.
22. Yavin, E., and Z. Yavin. 1974. Attachment and culture of dissociated cells from rat embryo cerebral hemispheres on polylysine-coated surface. *J. Cell Biol.* 62:540–546.
23. Tamba, Y., H. Ariyama, …, M. Yamazaki. 2010. Kinetic pathway of antimicrobial peptide magainin 2-induced pore formation in lipid membranes. *J. Phys. Chem. B.* 114:12018–12026.
24. Fuertes, G., A. J. García-Sáez, …, J. Salgado. 2010. Pores formed by Baxα5 relax to a smaller size and keep at equilibrium. *Biophys. J.* 99:2917–2925.
25. Berg, H. C., and E. M. Purcell. 1977. Physics of chemoreception. *Biophys. J.* 20:193–219.
26. Baltz, R. H. 2007. Antimicrobials from actinomycetes. *Microbe.* 2:125–131.
27. Hachmann, A. B., E. Sevim, …, J. D. Helmann. 2011. Reduction in membrane phosphatidylglycerol content leads to daptomycin resistance in *Bacillus subtilis*. *Antimicrob. Agents Chemother.* 55:4326–4337.
28. Oursel, D., C. Loutelier-Bourhis, …, C. M. Lange. 2007. Lipid composition of membranes of *Escherichia coli* by liquid chromatography/tandem mass spectrometry using negative electrospray ionization. *Rapid Commun. Mass Spectrom.* 21:1721–1728.
29. Gidden, J., J. Denson, …, J. O. Lay. 2009. Lipid compositions in *Escherichia coli* and *Bacillus subtilis* during growth as determined by MALDI-TOF and TOF/TOF mass spectrometry. *Int. J. Mass Spectrom.* 283:178–184.
30. Chen, Y. F., T. L. Sun, …, H. W. Huang. 2014. Interaction of daptomycin with lipid bilayers: a lipid extracting effect. *Biochemistry.* 53:5384–5392.
31. Kwok, R., and E. Evans. 1981. Thermoelasticity of large lecithin bilayer vesicles. *Biophys. J.* 35:637–652.
32. Boman, H. G., and D. Hultmark. 1987. Cell-free immunity in insects. *Annu. Rev. Microbiol.* 41:103–126.
33. Zasloff, M. 1987. Magainins, a class of antimicrobial peptides from *Xenopus* skin: isolation, characterization of two active forms, and partial cDNA sequence of a precursor. *Proc. Natl. Acad. Sci. USA.* 84:5449–5453.
34. Wade, D., A. Boman, …, R. B. Merrifield. 1990. All-D amino acid-containing channel-forming antibiotic peptides. *Proc. Natl. Acad. Sci. USA.* 87:4761–4765.

35. Pogliano, J., N. Pogliano, and J. A. Silverman. 2012. Daptomycin-mediated reorganization of membrane architecture causes mislocalization of essential cell division proteins. *J. Bacteriol.* 194:4494–4504.

36. Roversi, D., V. Luca, …, L. Stella. 2014. How many antimicrobial peptide molecules kill a bacterium? The case of PMAP-23. *ACS Chem. Biol.* 9:2003–2007.

37. Habermann, E. 1972. Bee and wasp venoms. *Science.* 177:314–322.

38. Dawson, C. R., A. F. Drake, …, R. C. Hider. 1978. The interaction of bee melittin with lipid bilayer membranes. *Biochim. Biophys. Acta.* 510:75–86.

39. Terwilliger, T. C., L. Weissman, and D. Eisenberg. 1982. The structure of melittin in the form I crystals and its implication for melittin's lytic and surface activities. *Biophys. J.* 37:353–361.

40. Dempsey, C. E. 1990. The actions of melittin on membranes. *Biochim. Biophys. Acta.* 1031:143–161.

41. Yang, L., T. A. Harroun, …, H. W. Huang. 2001. Barrel-stave model or toroidal model? A case study on melittin pores. *Biophys. J.* 81:1475–1485.

42. Sansom, M. S. 1991. The biophysics of peptide models of ion channels. *Prog. Biophys. Mol. Biol.* 55:139–235.

43. Turner, J., Y. Cho, …, R. I. Lehrer. 1998. Activities of LL-37, a cathelin-associated antimicrobial peptide of human neutrophils. *Antimicrob. Agents Chemother.* 42:2206–2214.

44. He, K., S. J. Ludtke, …, H. W. Huang. 1996. Neutron scattering in the plane of membranes: structure of alamethicin pores. *Biophys. J.* 70:2659–2666.

45. Qian, S., W. Wang, …, H. W. Huang. 2008. Structure of the alamethicin pore reconstructed by x-ray diffraction analysis. *Biophys. J.* 94:3512–3522.

46. Lee, M. T., T. L. Sun, …, H. W. Huang. 2013. Process of inducing pores in membranes by melittin. *Proc. Natl. Acad. Sci. USA.* 110:14243–14248.

47. Lee, C. C., Y. Sun, …, H. W. Huang. 2011. Transmembrane pores formed by human antimicrobial peptide LL-37. *Biophys. J.* 100:1688–1696.

48. Diez-Gonzalez, F., and J. B. Russell. 1997. Effects of carbonylcyanide-m-chlorophenylhydrazone (CCCP) and acetate on *Escherichia coli* O157:H7 and K-12: uncoupling versus anion accumulation. *FEMS Microbiol. Lett.* 151:71–76.

49. Chapple, D. S., D. J. Mason, …, R. W. Evans. 1998. Structure-function relationship of antibacterial synthetic peptides homologous to a helical surface region on human lactoferrin against *Escherichia coli* serotype O111. *Infect. Immun.* 66:2434–2440.

50. Piddock, L. J., Y. F. Jin, …, A. E. Asuquo. 1999. Quinolone accumulation by *Pseudomonas aeruginosa*, *Staphylococcus aureus* and *Escherichia coli*. *J. Antimicrob. Chemother.* 43:61–70.

51. Shai, Y. 1999. Mechanism of the binding, insertion and destabilization of phospholipid bilayer membranes by α-helical antimicrobial and cell non-selective membrane-lytic peptides. *Biochim. Biophys. Acta.* 1462:55–70.

52. Bechinger, B., and K. Lohner. 2006. Detergent-like actions of linear amphipathic cationic antimicrobial peptides. *Biochim. Biophys. Acta.* 1758:1529–1539.

53. Wimley, W. C., and K. Hristova. 2011. Antimicrobial peptides: successes, challenges and unanswered questions. *J. Membr. Biol.* 239:27–34.

54. Last, N. B., and A. D. Miranker. 2013. Common mechanism unites membrane poration by amyloid and antimicrobial peptides. *Proc. Natl. Acad. Sci. USA.* 110:6382–6387.

55. Melo, M. N., R. Ferre, and M. A. Castanho. 2009. Antimicrobial peptides: linking partition, activity and high membrane-bound concentrations. *Nat. Rev. Microbiol.* 7:245–250.

56. Matsuzaki, K., O. Murase, …, K. Miyajima. 1996. An antimicrobial peptide, magainin 2, induced rapid flip-flop of phospholipids coupled with pore formation and peptide translocation. *Biochemistry.* 35:11361–11368.

57. Ludtke, S. J., K. He, …, H. W. Huang. 1996. Membrane pores induced by magainin. *Biochemistry.* 35:13723–13728.

58. Qian, S., W. Wang, …, H. W. Huang. 2008. Structure of transmembrane pore induced by Bax-derived peptide: evidence for lipidic pores. *Proc. Natl. Acad. Sci. USA.* 105:17379–17383.

59. Williams, R. W., R. Starman, …, D. Covell. 1990. Raman spectroscopy of synthetic antimicrobial frog peptides magainin 2a and PGLa. *Biochemistry.* 29:4490–4496.

60. Matsuzaki, K., M. Harada, …, K. Miyajima. 1991. Physicochemical determinants for the interactions of magainins 1 and 2 with acidic lipid bilayers. *Biochim. Biophys. Acta.* 1063:162–170.

61. Matsuzaki, K., O. Murase, …, K. Miyajima. 1994. Orientational and aggregational states of magainin 2 in phospholipid bilayers. *Biochemistry.* 33:3342–3349.

62. Hirsh, D. J., J. Hammer, …, J. Schaefer. 1996. Secondary structure and location of a magainin analogue in synthetic phospholipid bilayers. *Biochemistry.* 35:12733–12741.

63. Bechinger, B., Y. Kim, …, S. J. Opella. 1991. Orientations of amphipathic helical peptides in membrane bilayers determined by solid-state NMR spectroscopy. *J. Biomol. NMR.* 1:167–173.

64. Gazit, E., W. J. Lee, …, Y. Shai. 1994. Mode of action of the antibacterial cecropin B2: a spectrofluorometric study. *Biochemistry.* 33:10681–10692.

65. Gazit, E., A. Boman, …, Y. Shai. 1995. Interaction of the mammalian antibacterial peptide cecropin P1 with phospholipid vesicles. *Biochemistry.* 34:11479–11488.

66. Schümann, M., M. Dathe, …, M. Bienert. 1997. The tendency of magainin to associate upon binding to phospholipid bilayers. *Biochemistry.* 36:4345–4351.

67. Strandberg, E., P. Wadhwani, …, A. S. Ulrich. 2006. Solid-state NMR analysis of the PGLa peptide orientation in DMPC bilayers: structural fidelity of ^{2}H-labels versus high sensitivity of ^{19}F-NMR. *Biophys. J.* 90:1676–1686.

68. Huang, H. W. 2000. Action of antimicrobial peptides: two-state model. *Biochemistry.* 39:8347–8352.

69. Huang, H. W., F. Y. Chen, and M. T. Lee. 2004. Molecular mechanism of peptide induced pores in membranes. *Phys. Rev. Lett.* 92:198304.

70. Litster, J. D. 1975. Stability of lipid bilayers and red blood cell membranes. *Phys. Lett. A.* 53:193–194.

71. Taupin, C., M. Dvolaitzky, and C. Sauterey. 1975. Osmotic pressure induced pores in phospholipid vesicles. *Biochemistry.* 14:4771–4775.

72. Adamson, A. W., and A. P. Gast. 1997. Physical Chemistry of Surfaces. John Wiley & Sons, Hoboken, NJ, pp. 6–8.

73. Brochard, F., P. G. Degennes, and P. Pfeuty. 1976. Surface-tension and deformations of membrane structures—relation to 2-dimensional phase-transitions. *J. Phys. (Paris).* 37:1099–1104.

74. Schneider, M. B., J. T. Jenkins, and W. W. Webb. 1984. Thermal fluctuations of large quasi-spherical bimolecular phospholipid-vesicles. *J. Phys. (Paris).* 45:1457–1472.

75. Strahl, H., F. Bürmann, and L. W. Hamoen. 2014. The actin homologue MreB organizes the bacterial cell membrane. *Nat. Commun.* 5:3442.

76. He, K., S. J. Ludtke, …, D. L. Worcester. 1995. Antimicrobial peptide pores in membranes detected by neutron in-plane scattering. *Biochemistry.* 34:15614–15618.